Density Functional Theory Study of the Mechanisms of Iron-Catalyzed Intramolecular C−H Amination [1,2]-Shift Tandem Reactions of Aryl Azides

ARTICLE *in* ORGANOMETALLICS · MARCH 2015

Impact Factor: 4.13 · DOI: 10.1021/acs.organomet.5b00087

4 AUTHORS, INCLUDING:

Qinghua Ren

Shanghai University

29 PUBLICATIONS **222** CITATIONS

SEE PROFILE

Jianhui Fang

Shanghai University

48 PUBLICATIONS **845** CITATIONS

SEE PROFILE

ORGANOMETALLICS

Article

pubs.acs.org/Organometallics

Density Functional Theory Study of the Mechanisms of Iron-Catalyzed Intramolecular C−H Amination [1,2]-Shift Tandem Reactions of Aryl Azides

Qinghua Ren,* Xiaoyan Shen, Jinyu Wan, and Jianhui Fang

Department of Chemistry, Innovative Drug Research Center, Shanghai University, 99 Shangda Road, Shanghai 200444, China

Supporting Information

ABSTRACT: The mechanisms of iron(II) bromide-catalyzed intramolecular C−H bond amination [1,2]-shift tandem reactions of aryl azides have been studied using density functional theory calculations. The tandem reaction from $\mathbf{R_1}$, 1-azido-2-(1-methoxy-2-methylpropan-2-yl)benzene, to produce $\mathbf{P_2}$, 2,3-dimethyl-1*H*-indole, was calculated. Our results showed that the overall catalytic cycle includes the following steps: (I) extrusion of N_2 to form iron nitrene; (II) C−H bond amination; (III) formation of the middle product $\mathbf{P_1}$, 2-methoxy-3,3-dimethylindoline; (IV) iminium ion formation ; (V) [1,2]-shift process; and (VI) formation of indole $\mathbf{P_2}$. The rate-limiting step is the [1,2]-shift process, where the energy barrier ΔE = 28.7 kcal/mol in the gas phase. Our calculated results also indicated that the preference for the [1,2]-shift component of the tandem reaction is methyl < ethyl.

1. INTRODUCTION

It is well known that transition-metal catalysts are essential for the formation of carbon−carbon and carbon−heteroatom bonds in modern organic synthesis.[1−4] However, most of them are limited by the high price or considerable toxicity, especially in the context of manufacturing on larger scales. Therefore, the inexpensive, nontoxic first-row transition metal iron has recently been paid more attention.[5−10]

Transition-metal-catalyzed C−H bond amination has been developed as a useful synthetic process.[11−17] It can be incorporated into cascade reactions to rapidly increase the molecular complexity of simple substrates. In recent years, metal catalysts such as Ru,[18−20] Rh,[21−23] Co,[24,25] Ir,[26−28] and Zn[29] have been reported to display valid activity toward the formation of new C−N bonds from vinyl or aryl C−H bonds. Azides are used as the N atom source. These are environmentally friendly N-atom-transfer reactions because no oxidant is required and the only byproduct is environmentally benign N_2 gas.[30−32]

However, these transformations often require electron-withdrawing groups on the azides.[33] It seems that it is more interesting and challenging to use electron-neutral aryl azides as the N atom source. Driver's group first used rhodium(II) dicarboxylate complexes as precatalysts and aryl azides as the N atom precursor.[34] They found that both electron-rich and electron-poor aryl azides are efficient sources for aliphatic C−H bond amination reactions. The same group then developed an iron(II) bromide-catalyzed ethereal C−H bond amination 1,2-migration tandem reaction,[35] which could efficiently and selectively transform ortho-substituted aryl azides into 2,3-disubstituted indoles. Iron(II) bromide is commercially available, cheap, nontoxic, and air and moisture stable, and it can be easily prepared and modified.

Driver's discovery of this iron-catalyzed C−H bond amination [1,2]-shift tandem reaction of aryl azides[35] is an important synthetic advancement. However, the group did not theoretically investigate the mechanisms of these reactions, although they gave a mechanistic proposal, shown in Scheme 1.

Is it a proper mechanism? Is the mechanism of iron(II) bromide-catalyzed intramolecular C−H bond amination consistent with the mechanisms of other metal catalysts? Li's group[36] has theoretically studied the intramolecular C−H amination reaction mechanisms of biaryl azides catalyzed by (cod)Ir(OMe), $RuCl_3$, $Rh_2(O_2CCF_3)_4$, and ZnI_2. Their

Scheme 1. Mechanistic Proposal for the Iron-Catalyzed [1,2]-Shift Tandem Reaction

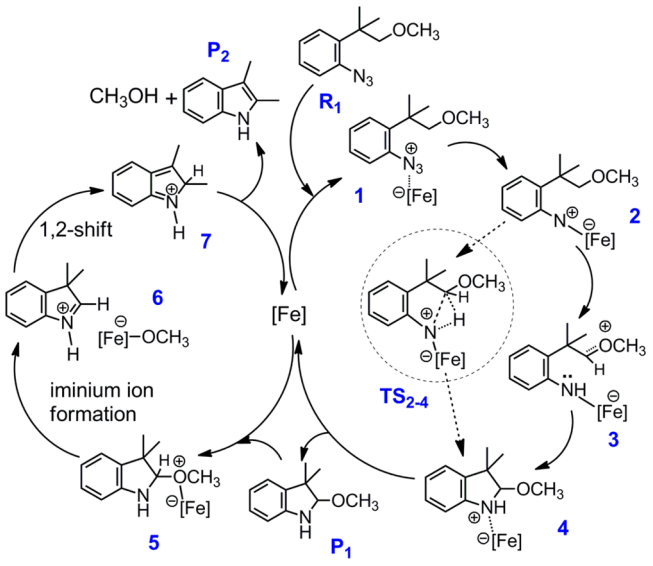

Received: January 30, 2015
Published: March 5, 2015

DOI: 10.1021/acs.organomet.5b00087
Organometallics 2015, 34, 1129−1136

calculated results showed that the C−H amination reactions mainly proceeded through a stepwise mechanism: nitrogen liberation followed by formation of a C−N bond and then 1,2-hydrogen shift. Does this conclusion fit for the iron(II) bromide-catalyzed C−H bond amination 1,2-migration tandem reaction? It will be valuable to perform computational studies to explore the mechanisms of these kinds of reactions.

On the basis of the experimental work of Driver,[35] we selected one typical of reaction for our model calculation, which is shown in Scheme 2. The reactant is 1-azido-2-(1-methoxy-2-methylpropan-2-yl)benzene, named $\mathbf{R_1}$. The corresponding products are $\mathbf{P_1}$ and $\mathbf{P_2}$.[35] The possible mechanisms for the catalytic cycles of the reaction were thoroughly investigated. We also studied the transfer preference between ethyl and methyl for the 1,2-shift process of the tandem reaction.

Scheme 2. Model Reaction of the Iron(II) Bromide-Catalyzed [1,2]-Shift Tandem Reaction

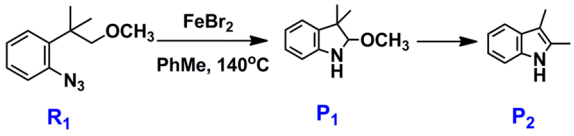

We used density functional theory (DFT) calculations with the B3LYP method[37−40] to gain insight into the mechanisms of iron(II) bromide-catalyzed intramolecular C−H bond amination [1,2]-shift tandem reactions. Our calculations try to answer these questions: How does each of the catalytic steps take place? Which step is the rate-determining step in the whole catalytic cycle? Which is favored, methyl or ethyl, in the [1,2]-shift process? Is it possible to proceed via mechanisms different from those of suggested by Driver's group, shown in Scheme 1? Answers to these questions will improve the understanding of these kinds of iron-catalyzed intramolecular C−H bond amination [1,2]-shift Tandem reactions of aryl azides.

2. COMPUTATIONAL DETAILS

All calculations were performed using DFT with the B3LYP hybrid functional.[37−40] The 6-31g(d,p) basis set was used for C, H, O, and N, and the 6-311g** basis set was selected for Br.[41,42] The SDD quasi-relativistic pseudopotential and associated basis set were used for Fe.[43] The gas-phase geometries of all intermediates and transition states were fully optimized without any symmetry restriction, following the vibrational frequencies analysis to ensure that the local minima had zero imaginary frequencies and the transition state had exactly one. The C-PCM polarizable conductor calculation model[44] with the UFF radii on the gas-phase-optimized geometries of single points was used to calculate the solvation effect in toluene. Both the electronic and nonelectronic free energies in solution were added to the gas-phase Gibbs free energies to obtain the solution Gibbs free energies in toluene, ΔG_{sol}. All calculations were implemented in the Gaussian 03 program.[45]

3. RESULTS AND DISCUSSION

3.1. Mechanisms of Cycle A without Passing through the Middle Product P_1. According to the mechanistic proposal shown in Scheme 1, suggested by Driver's and Li's groups,[35,36] we found several possible mechanisms for the model reaction shown in Scheme 2. One path that does not pass through the middle product $\mathbf{P_1}$ to get to the final product $\mathbf{P_2}$ was named as Cycle A. The full catalytic cycle of the mechanisms for Cycle A is outlined in Figure 1, and its energy profiles are shown in Figure 2. All of the optimized structures are shown in Figure S1 in the Supporting Information.

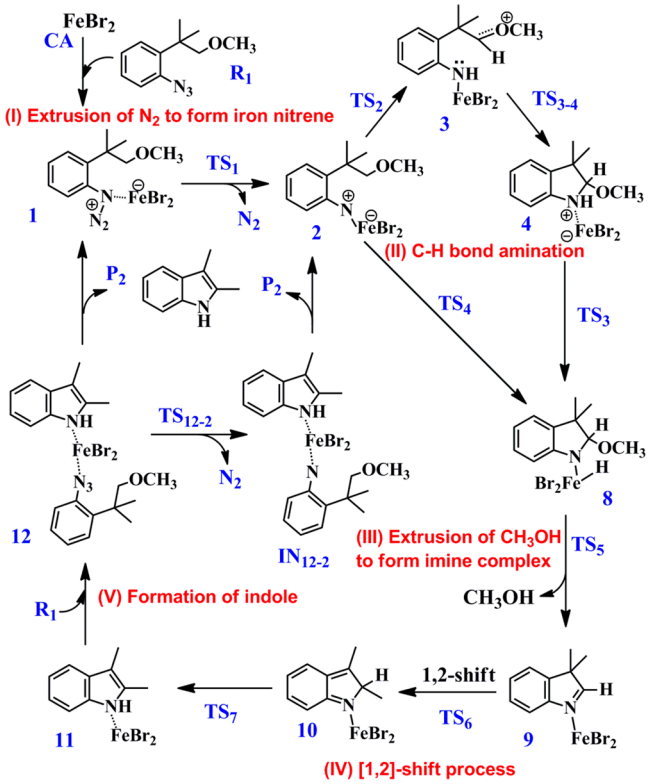

Figure 1. Outline of the iron(II) bromide-catalyzed mechanisms of Cycle A.

The overall catalytic cycle of the mechanism for Cycle A without passing through the middle product $\mathbf{P_1}$ to get the final product $\mathbf{P_2}$ includes several basic steps:

(I) *Extrusion of N_2 to form iron nitrene.* The approach of the aryl azide, $\mathbf{R_1}$, toward the catalyst **CA**, $FeBr_2$, leads to the formation of the complex, **1**. From **1**, passing through the transition state $\mathbf{TS_1}$, the iron nitrene, **2** is formed while releasing the N_2 gas. The energy barrier of $\mathbf{TS_1}$ is 21.2 kcal/mol where the electronic energy of the complex **1** is set as zero energy. From the optimized structures of them (see Figure S1 in the Supporting Information), we can see that the distance of Fe−N is 1.99 Å in **1**. It becomes short to 1.79 Å in $\mathbf{TS_1}$ and 1.58 Å in **2**. The iron nitrene structure is formed in **2**. The bonding of C−N decreases to 1.35 Å (compared to 1.44 Å in $\mathbf{TS_1}$ and 1.48 Å in **1**). This step is similar as the mechanistic proposal shown in Scheme 1 suggested by Driver.[35]

(II) *C−H bond amination.* The C−H bond amination reaction has two possibilities. One way is the concerted mechanism from **2** to **8** passing through the transition state $\mathbf{TS_4}$, where the carbon atom in **2** connects with the N atom while one H atom from the carbon atom goes to combine with the iron atom directly to form **8**. The distance of C−N is 3.12 Å in **2** and becomes short to 2.64 Å in $\mathbf{TS_4}$ and 1.51 Å in **8**. At the same time, the H−Fe bond is formed (1.44 Å in **8**, compared to 1.50 Å in $\mathbf{TS_4}$ and 3.02 Å in **2**). However, the distance of H−N is 2.36 Å in **8**, which means the H atom is moved from C atom to connect Fe atom, but not to combine with N atom. The energy barrier of the concerted transition state $\mathbf{TS_4}$ is 11.0 kcal/mol. Another way is a three-step stepwise

DOI: 10.1021/acs.organomet.5b00087
Organometallics 2015, 34, 1129−1136

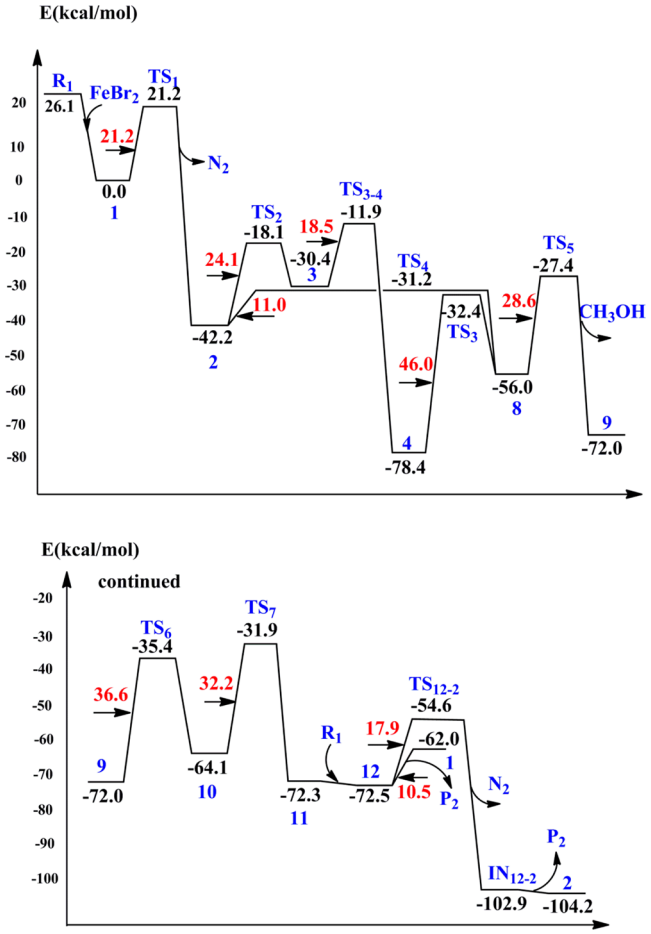

Figure 2. Energy profiles for the mechanisms of Cycle A (energies in kcal/mol).

process. One H atom in **2** intermediate transfers from the carbon atom to the N atom to form the oxocarbenium ion **3** after passing through the transition state $\mathbf{TS}_2$. The oxocarbenium ion **3** intermediate was proposed by Driver.[35] The bonding of H−N is 1.01 Å in **3** (compared to 1.23 Å in $\mathbf{TS}_2$). Then, the H atom of **3** connecting with the N atom moves around the N center to make the N atom combined with the C atom to form **4** after passing through the transition state $\mathbf{TS}_{3-4}$. The C−N bond is formed in **4** (1.53 Å compared to 2.53 Å in $\mathbf{TS}_{3-4}$, and 3.09 Å in **3**). It can also be seen that the distance of N−Fe becomes longer to 1.97 Å in **4** (compared to 1.58 Å in **2** and 1.89 Å in **3**), which means the N−Fe bond has already become weak in **4**. Then, **4** could form the intermediate **8** when the H atom transfers from the N atom to the Fe atom passing through the transition state $\mathbf{TS}_3$. The distance of H−N becomes longer to 1.50 Å in $\mathbf{TS}_3$ and 2.36 Å in **8** from 1.03 Å in **4**. From Figure 2, it can be seen that the energy barrier of $\mathbf{TS}_2$ from **2** to obtain **3** is 24.1 kcal/mol and the energy barrier of $\mathbf{TS}_{3-4}$ from **3** to form **4** is 18.5 kcal/mol. But the energy barrier of $\mathbf{TS}_3$ from **4** to form **8** is 46.0 kcal/mol, which is too high. The intermediate **4** was proposed by Driver et al.[35] From **2** to **8**, the energy barrier of $\mathbf{TS}_4$ (11.0 kcal/mol) is much smaller than that of $\mathbf{TS}_2$ (24.1 kcal/mol), $\mathbf{TS}_{3-4}$ (18.5 kcal/mol) and $\mathbf{TS}_3$ (46.0 kcal/mol), which means the process passing through the concerted transition state $\mathbf{TS}_4$ to obtain **8** directly from **2** is favored. The intermediate **8** is an iron(IV) hydride, which was not proposed by Driver et al.[35] As far as we know, some iron(IV) hydride species have been reported, such as, $[Cp^*Fe(dppe)(H)_2]^+$ (dppe = bis(diphenylphosphino)-ethane),[46] (η^6-arene)$Fe(H)_2(SiCl_3)_2$,[47] $[Fe(H)_3(Pet_3)_4]^+$,[48] etc. In the mechanism studies of Peters,[49] the iron(IV) hydride species $[PhBP^{iPr}_3]Fe(H)_3(PR_3)$ (PR_3=PMe_3, PEt_3, or $PMePh_2$) were included in the catalytic cycles.

(III) *Extrusion of CH_3OH to form imine complex.* After the intermediate **8** is formed, the H atom of Fe will combine with the methoxy carbon to release CH_3OH molecule. This process is passing through the transition state $\mathbf{TS}_5$ to form **9**. The distance of H−O is 1.79 Å in $\mathbf{TS}_5$ (compared to 2.56 Å in **8**), while the distances of C−O and Fe−H become longer to 2.07, 1.46 Å in $\mathbf{TS}_5$ compared to 1.38, 1.44 Å in **8**, respectively. We also can see that the double N=C bond is formed in **9** (The distance of N−^{1}C is 1.29 Å, compared to 1.33 in $\mathbf{TS}_5$ and 1.51 Å in **8**). The energy barrier of $\mathbf{TS}_5$ is 28.6 kcal/mol.

(IV) *[1,2]-Shift process.* The methyl of ^{2}C in **9** is shifted to ^{1}C to form **10** after passing through the transition state $\mathbf{TS}_6$, where the energy barrier of $\mathbf{TS}_6$ is 36.6 kcal/mol. From the optimized structures in the Supporting Information, it can be seen that the distance between the ^{3}C atom of the transferring methyl and ^{2}C atom increases from 1.55 Å in **9** to 2.01 Å in $\mathbf{TS}_6$ and 2.55 Å in **10**. At the same time, the bond between the ^{3}C atom of the transferring methyl and ^{1}C atom is formed in **10** (1.54 Å, compare to 1.90 Å in $\mathbf{TS}_6$ and 2.51 Å in **9**).

(V) *Formation of indole.* The remaining H atom of ^{1}C in **10** is transferred from the ^{1}C atom to the N atom to form **11**. The transition state from **10** to **11** is $\mathbf{TS}_7$, which energy barrier is 32.2 kcal/mol. The bond of H−N is formed in **11** (1.02 Å, compared to 1.31 Å in $\mathbf{TS}_7$). At the same time, the bonding of N−Fe becomes longer to 2.02 Å in **11** (compared to 1.93 Å in $\mathbf{TS}_7$). From **11**, the approach of $\mathbf{R}_1$ toward the $FeBr_2$ part of **11** leads to form the complex **12** and then it returns to **1** while generating the final product $\mathbf{P}_2$, 2,3-dimethyl-1*H*-indole. The energy needs 10.5 kcal/mol. It is also possible that the complex **12** goes to the intermediate $\mathbf{IN}_{12-2}$ after passing through the transition state $\mathbf{TS}_{12-2}$ while releasing the N_2 gas. Then $\mathbf{IN}_{12-2}$ returns to **2** while generating the final product $\mathbf{P}_2$. The energy barrier of $\mathbf{TS}_{12-2}$ is 17.9 kcal/mol, which is higher than the needed energy (10.5 kcal/mol) from **12** to **1**.

From Figure 2, it can be seen that the energy barrier from **9** to obtain **10** (36.6 kcal/mol for $\mathbf{TS}_6$) is higher than the others (21.2 kcal/mol for $\mathbf{TS}_1$; 11.0 kcal/mol for $\mathbf{TS}_4$; 28.6 kcal/mol for $\mathbf{TS}_5$; 32.2 kcal/mol for $\mathbf{TS}_7$). This means that the rate-limiting step for the whole catalytic cycles of Cycle A without passing through the middle product $\mathbf{P}_1$ to get the final product $\mathbf{P}_2$ of the model reaction is [1,2]-shift process, in which the energy barrier of $\mathbf{TS}_6$ is 36.6 kcal/mol.

3.2. Mechanisms of Cycle B with Passing through the Middle Product $\mathbf{P}_1$. Following the mechanistic proposal shown in Scheme 1, suggested by Driver,[35] we studied the path of Cycle B that does pass through the middle product $\mathbf{P}_1$ to obtain the final product $\mathbf{P}_2$. The full catalytic cycle of the mechanisms for Cycle B is outlined in Figure 3, and its energy profiles are shown in Figure 4. All of the optimized structures are shown in Figure S1 in the Supporting Information.

The first step of the catalytic cycle is the extrusion of N_2 to form iron nitrene, which is the same as step (I) of Cycle A shown in Figure 1. The energy barrier of $\mathbf{TS}_1$ is 21.2 kcal/mol. But the following steps are different:

(II) *C−H bond amination.* The C−H bond amination reaction from **2** to **4** has several possibilities. One way is the hydride-transfer mechanism suggested by Driver,[35] which passes through the double-radical intermediate **3** shown in

DOI: 10.1021/acs.organomet.5b00087
Organometallics 2015, 34, 1129−1136

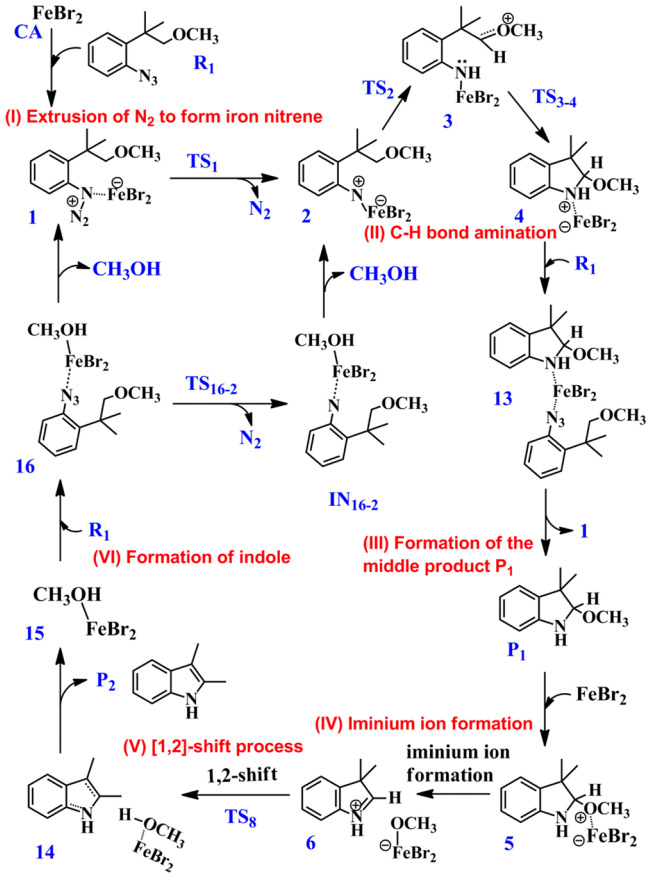

Figure 3. Outline of the iron(II) bromide-catalyzed mechanisms of Cycle B.

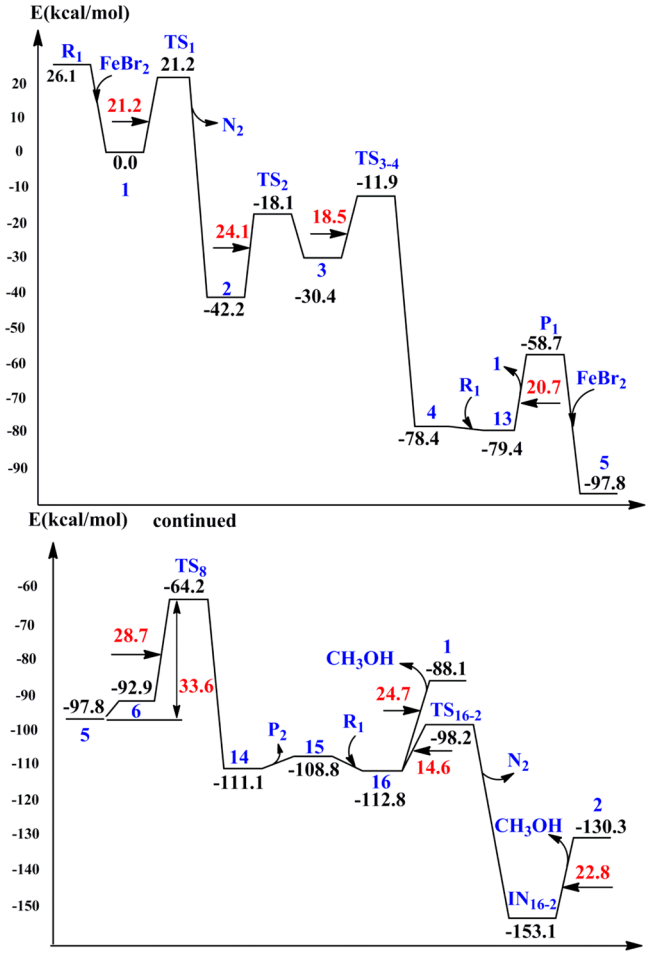

Figure 4. Energy profiles for the mechanisms of Cycle B (energies in kcal/mol).

Figure 3. The hydride-transfer mechanism for C−H bond functionalization was generally accepted.[50−52] The energy barriers of $\mathbf{TS_2}$ from **2** to **3** and of $\mathbf{TS_{3\text{-}4}}$ from **3** to **4** for the hydride-transfer mechanism are 24.1 and 18.5 kcal/mol, respectively (see Figure 4). Another possibility is a concerted mechanism from **2** to **4**, where one H atom in **2** transfers from the carbon atom to the N atom accompanying the formation of a C−N bond to form **4**. We did not get the concerted transition state from **2** to **4**. This seems that another two-step stepwise process is more possible, including the first step from **2** to **8** (passing through the concerted transition state $\mathbf{TS_4}$, 11.0 kcal/mol) and the second step from **8** to **4** (passing through the back way of $\mathbf{TS_3}$, 23.6 kcal/mol), which means the H atom could go to Fe first and then to the N atom (see Figure 2). The energy barriers for these two pathways (from **2** to **3** then to **4**, or from **2** to **8** then to **4**) are similar.

(III) *Formation of the middle product* $\mathbf{P_1}$. Approach of the aryl azide, $\mathbf{R_1}$, toward the $FeBr_2$ part of **4** leads to the formation of the complex **13**, which then returns to **1** while generating the middle product $\mathbf{P_1}$, 2-methoxy-3,3-dimethylindoline. The energy needed is 20.7 kcal/mol. The structure of **13** also likes the complex formed by $\mathbf{P_1}$ and **1**. The distance of Fe−N (of $\mathbf{R_1}$ part) is 2.04 Å, and the distance of Fe−N (of $\mathbf{P_1}$ part) is 2.08 Å (cf. the distance of N−Fe in complex **1**, 1.99 Å). This process is similar to the mechanistic proposal suggested by Driver.[35]

(IV) *Iminium ion formation.* After $\mathbf{P_1}$ is formed, approach of the catalyst $FeBr_2$ toward $\mathbf{P_1}$ leads to the formation of complex **5**. Coordination of the Lewis acidic iron salt to the methyl ether promotes the generation of iminium ion **6**.[53,54] The energy required for the iminium ion formation step is 4.9 kcal/mol.

(V) *[1,2]-Shift process.* The methyl of ^2C in **6** is shifted to ^1C to form **14** after passing through the transition state $\mathbf{TS_8}$, while the H atom of ^1C goes to the O atom. From the optimized structures in the Supporting Information, it can be seen that the distance between the transferring H atom and O atom decreases from 1.89 Å in **6** to 0.99 Å in **14**. The H−O bond in **14** is formed. At the same time, the bond between the ^3C atom of the transferring methyl and the ^1C atom in **14** is formed (1.50 Å, cf. 1.89 Å in $\mathbf{TS_8}$ and 2.49 Å in **6**). The energy barrier of $\mathbf{TS_8}$ is 28.7 kcal/mol.

(VI) *Formation of indole* $\mathbf{P_2}$, *2,3-dimethyl-1H-indole.* From **14**, the final product $\mathbf{P_2}$ is generated while releasing the complex **15**. The approach of $\mathbf{R_1}$ toward **15** then leads to the formation of complex **16**. Finally, extrusion of CH_3OH from **16** returns the complex **1**. The energy needed is 24.7 kcal/mol. It is also possible that complex **16** goes to the intermediate $\mathbf{IN_{16\text{-}2}}$ after passing through the transition state $\mathbf{TS_{16\text{-}2}}$ while releasing N_2 gas. The energy barrier of $\mathbf{TS_{16-2}}$ is 14.6 kcal/mol. Intermediate $\mathbf{IN_{16\text{-}2}}$ then returns to **2** while releasing the CH_3OH molecule. The energy needed is 22.8 kcal/mol, which is closer to the energy needed (24.7 kcal/mol) for going from **16** to **1**.

The overall catalytic cycle of the mechanism for Cycle B involves the following steps: (I) extrusion of N_2 to form iron nitrene; (II) C−H bond amination; (III) formation of the middle product $\mathbf{P_1}$; (IV) iminium ion formation; (V) [1,2]-shift

DOI: 10.1021/acs.organomet.5b00087
Organometallics 2015, 34, 1129−1136

process; and (VI) formation of indole $\mathbf{P_2}$ and extrusion of CH_3OH. From Figure 4, it can be seen that the rate-limiting step for the whole catalytic mechanism of Cycle B is also the [1,2]-shift process, where the energy barrier of $\mathbf{TS_8}$ is 28.7 kcal/mol. Compared to the values of Cycle A (see Figure 2), it can be seen that the energy barrier of $\mathbf{TS_8}$ (28.7 kcal/mol) for the rate-limiting step of Cycle B is smaller than that of $\mathbf{TS_6}$ (36.6 kcal/mol) for the rate-limiting step of Cycle A, which means the mechanism of Cycle B, passing through the middle product $\mathbf{P_1}$, is favored over the mechanism of Cycle A, which does not pass through the middle product $\mathbf{P_1}$. The calculated results prove that the mechanistic proposal suggested by Driver[35] is proper.

3.3. Solvent Effect. All the above calculations were implemented in the gas phase. To clarify whether solvent can have a significant effect on our calculated system, we calculated the Gibbs free energy in solvent PhMe for the overall catalytic mechanisms of Cycle A and Cycle B. All the solution-phase free energies in this article correspond to the reference state of 1 mol/L, 298 K.

The Gibbs free energies in the gas phase, ΔG, and in solvent PhMe, ΔG_{sol}, for the overall catalytic mechanism of Cycle A are shown in Figure 5. The former is depicted as the solid line, and the latter is drawn as the dashed line. We can see that the rate-limiting step in solvent PhMe is also the [1,2]-shift process when passing through the transition state $\mathbf{TS_6}$, where the ΔG_{sol} value in solvent PhMe is 33.1 kcal/mol and the solvation effect is not obvious (compared to the gas-phase ΔG = 36.0 kcal/mol).

Similarly, the Gibbs free energies in the gas phase, ΔG, and in solvent PhMe, ΔG_{sol}, for the overall catalytic mechanism of Cycle B are shown in Figure 6. It can be seen that the rate-limiting step in solvent PhMe for Cycle B is still the [1,2]-shift process when passing through the transition state $\mathbf{TS_8}$, where the ΔG_{sol} value in solvent PhMe is 26.8 kcal/mol, which is smaller than that for Cycle A (33.1 kcal/mol). It can be concluded that Cycle B is favored. The solvation effect does not change this conclusion. The mechanisms in the gas phase can be effectively used for the model reaction.

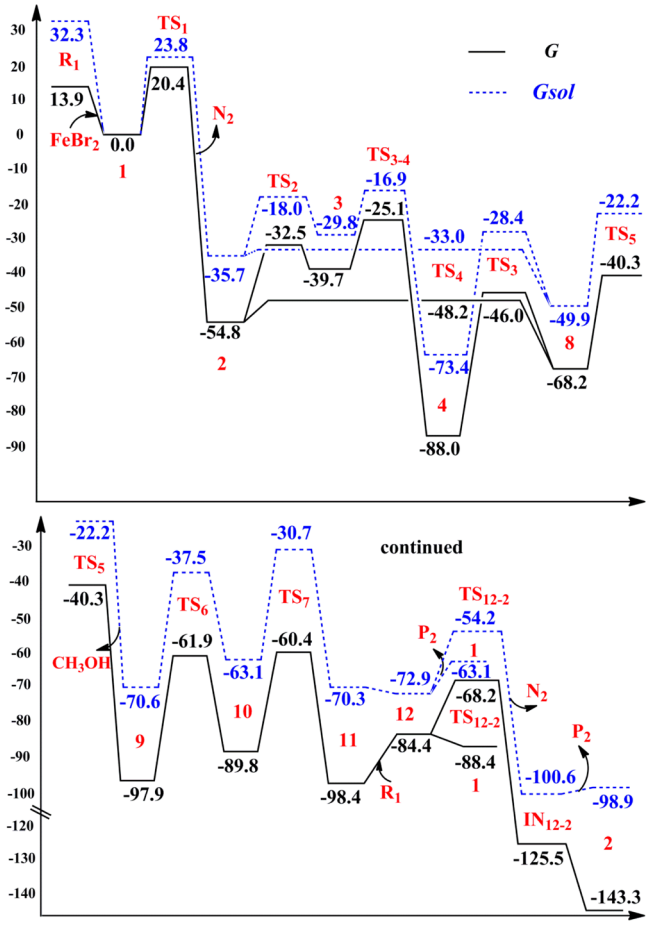

Figure 5. Gibbs free energies in the gas phase, ΔG (solid line), and in solvent PhMe, ΔG_{sol} (dashed line), for the overall catalytic mechanism of Cycle A (energies in kcal/mol).

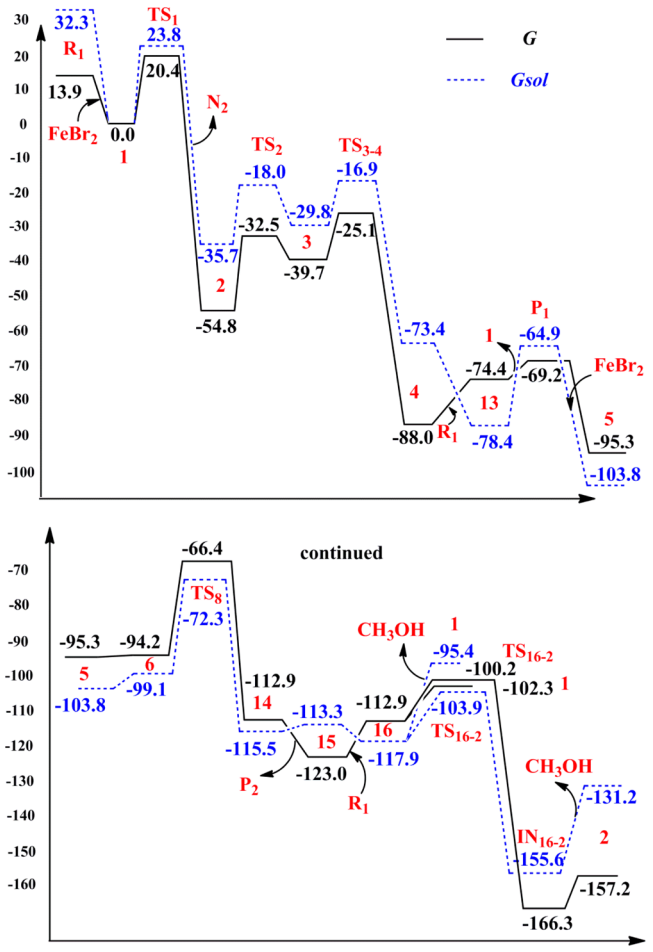

Figure 6. Gibbs free energies in the gas phase, ΔG (solid line), and in solvent PhMe, ΔG_{sol} (dashed line), for the overall catalytic mechanism of Cycle B (energies in kcal/mol).

3.4. Transferring Preference between Methyl and Ethyl for the [1,2]-Shift Process. If the two methyl parts of $\mathbf{R_1}$, 1-azido-2-(1-methoxy-2-methylpropan-2-yl)benzene, are changed so that one is different, such as one methyl and one ethyl, i.e., 1-azido-2-(1-methoxy-2-ethylpropan-2-yl)benzene, $\mathbf{R_2}$, the [1,2]-shift component of the calculated tandem reaction would show selectivity. We have investigated preference between transferring methyl and ethyl for the [1,2]-shift process. The [1,2]-shift steps for Cycle A and Cycle B are outlined in Figure 7, and the energy profiles are shown in Figure 8. All of the optimized structures are shown in Figure S1 in the Supporting Information. In Cycle B, the ethyl of **17** is

DOI: 10.1021/acs.organomet.5b00087
Organometallics 2015, 34, 1129−1136

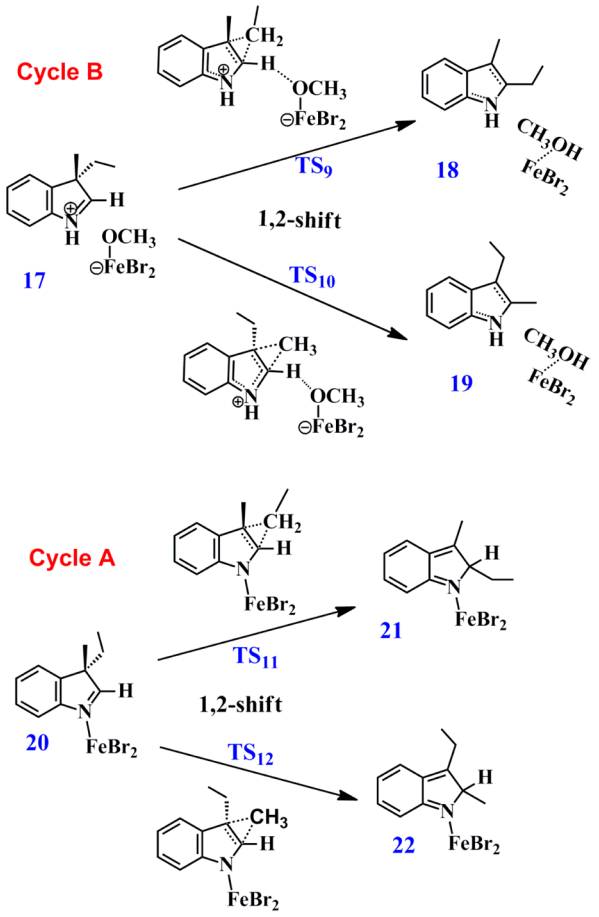

Figure 7. Outline of the [1,2]-shift steps for transferring methyl and ethyl for the catalytic cycles of Cycle A and Cycle B.

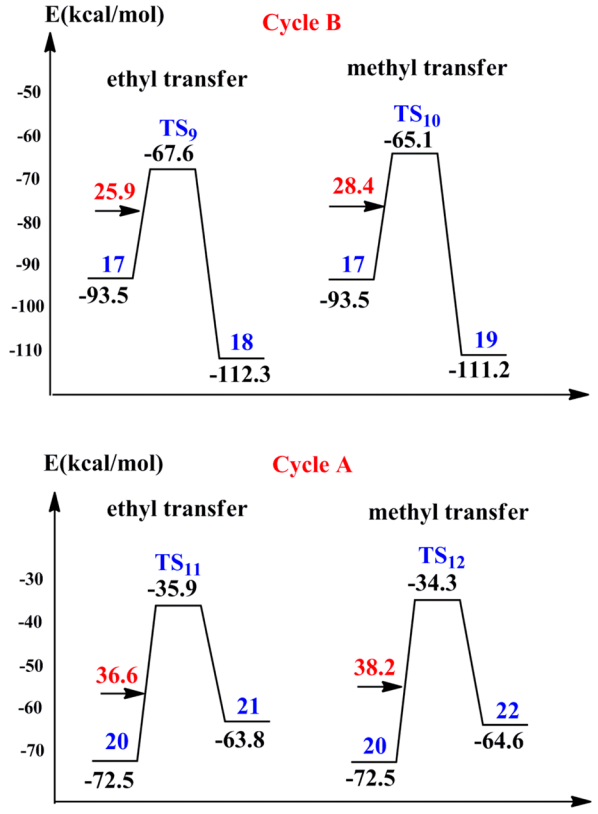

Figure 8. Energy profiles for the [1,2]-shift steps for transferring methyl and ethyl for the catalytic cycles of Cycle A and Cycle B (energies in kcal/mol).

transferred to form **18** after passing through the transition state TS_9, and the methyl of **17** is shifted to form to **19** after passing through the transition state TS_{10}. From Figure 8, it can be seen that TS_9 (25.9 kcal/mol) is smaller than TS_{10} (28.4 kcal/mol), which means that the migration preference is methyl < ethyl. This conclusion meets the experimental results reported by Driver.[35]

In Cycle A, the ethyl of **20** is transferred to form **21** after passing through the transition state TS_{11}, and the methyl of **20** is shifted to form **22** after passing through the transition state TS_{12}. From Figure 8, it can also be seen that TS_{11} (36.6 kcal/mol) is smaller than TS_{12} (38.2 kcal/mol), which also means that the migration preference is methyl < ethyl. The conclusion is the same.

One the other hand, we can see that the energy barrier of TS_{11} is higher than that of TS_9, and the energy barrier of TS_{12} is higher than that of TS_{10}, which means that Cycle B, which passes through the middle product P_1, is favored over Cycle A, which does not pass through the middle product P_1. The results also support that the mechanistic proposal suggested by Driver[35] is proper.

3.5. Ligand Effect. Ligand effect is always discussed in transition-metal-catalyzed coupling reactions.[55,56] Considering that methanol is formed as a byproduct in the catalytic cycles, we calculated whether iron alkoxides are involved in the cycles as the active catalyst. One or two methoxy ligands are used to replace the Br ligands to connect the iron center, and the corresponding transition states and intermediates are named as **a** or **b**, respectively.

First, the C−H amination steps from **2a** to **3a** via TS_{2a} and to **4a** for one Br and one methoxy ligands, or from **2b** to **3b** via TS_{2b} and to **4b** for two methoxy ligands, are calculated to compare the same steps from **2** to **3** via TS_2 and to **4** for two Br ligands. The energy profiles for **2a**, **4a**, TS_{2a}, **2b**, **4b**, and TS_{2b} are shown in Figure 9, and their optimized structures are shown in the Supporting Information. It can be seen that the energy barrier of TS_{2a} is 28.9 kcal/mol and that of TS_{2b} is 33.9 kcal/mol, both of which are much higher than that of TS_2 (24.1 kcal/mol, see Figure 2 or 4). This means that the methoxy ligand is not favored in the C−H amination step.

Next, we checked the ligand effect for the rate-limiting step of Cycle A. The calculated results from **9a** to **10a** via TS_{6a} for one Br and one methoxy ligands, or from **9b** to **10b** via TS_{6b} for two methoxy ligands, are also shown in Figure 9. It can be seen that the energy barriers of TS_{6a} and TS_{6b} are 38.1 and 39.5 kcal/mol, respectively, which are also higher than that of TS_6 (36.6 kcal/mol, see Figure 2). Thus, the methoxy ligand is also not favored in the rate-limiting step of Cycle A.

Finally, the ligand effect for the rate-limiting step of Cycle B was checked. The calculated results from **5a** to **14a** via **6a** and TS_{8a} for one Br and one methoxy ligands, or from **5b** to **14b** via **6b** and TS_{8b} for two methoxy ligands, are shown in Figure 9. It can be seen that the energy barrier from **5a** to TS_{8a} is 36.4 kcal/mol, which is higher than that from **5** to TS_8 (33.6 kcal/mol, see Figure 4). Similarly, the energy barrier from **5b** to TS_{8b} is 52.2 kcal/mol, which is much higher than 33.6 kcal/mol from **5** to TS_8. According to the model proposed by Shaik et al.,[57,58] the "energetic span" between the lowest and highest energy

DOI: 10.1021/acs.organomet.5b00087
Organometallics 2015, 34, 1129−1136

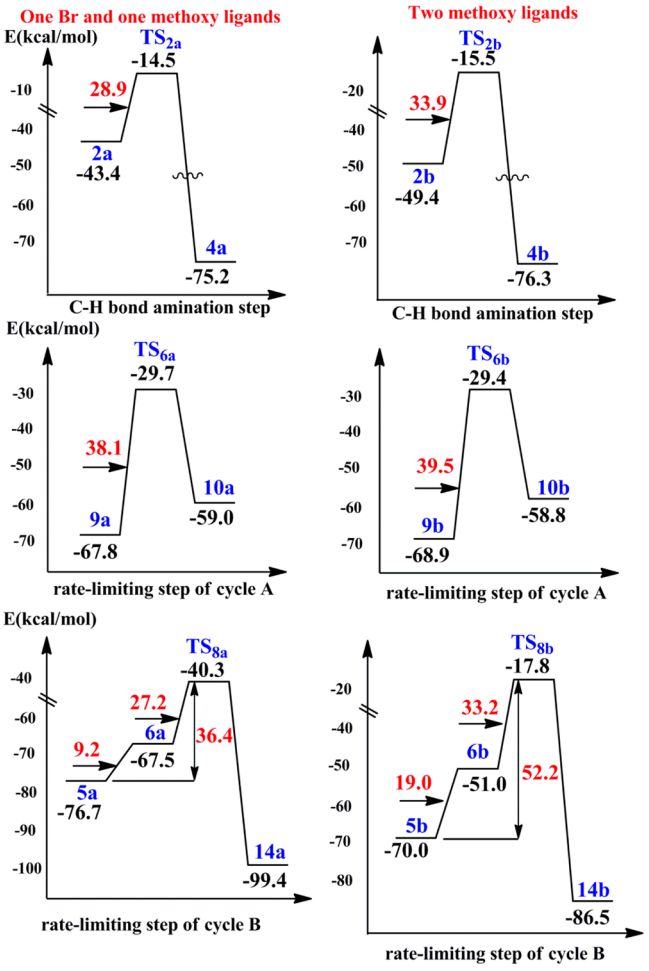

Figure 9. Energy profiles for the ligand effect of one Br and one methoxy or two methoxy ligands for the rate-limiting steps and C−H bond amination step (energies in kcal/mol).

species along the reaction path from **5a** passing through **6a** to obtain **14a**, or from **5b** passing through **6b** to obtain **14b**, is 59.1 or 68.7 kcal/mol, respectively, which is much higher than 46.9 kcal/mol from **5** passing through **6** to obtain **14** (see Figure 4). It can be concluded that the methoxy ligand is not favored over the Br ligand in the rate-limiting step of Cycle B. In all, it is appropriate to use two Br ligands connecting the Fe center in the above calculations.

4. CONCLUSION

The present paper thoroughly investigated the mechanisms of iron(II) bromide-catalyzed intramolecular C−H bond amination [1,2]-shift tandem reactions of aryl azides using DFT calculations with B3LYP method. The tandem reaction from $\mathbf{R_1}$ to produce $\mathbf{P_1}$ and $\mathbf{P_2}$ was calculated. We studied two different mechanisms, Cycle A which does not pass through the middle product $\mathbf{P_1}$, and Cycle B which does pass through the middle product $\mathbf{P_1}$. The rate-limiting step for both mechanisms is the [1,2]-shift process. Our results showed that the mechanism of Cycle B is favored over that of Cycle A, where the energy barrier for the rate-limiting step of the former is 28.7 kcal/mol and that of the latter is 36.6 kcal/mol, which proved that the mechanistic proposal suggested by Driver's group[35] is proper. The overall catalytic mechanism of the favored Cycle B includes the following basic steps: (I) extrusion of N_2 to form iron nitrene; (II) C−H bond amination; (III) formation of the middle product $\mathbf{P_1}$; (IV) iminium ion formation; (V) [1,2]-shift process; and (VI) formation of indole $\mathbf{P_2}$ and extrusion of CH_3OH. Our calculated results also indicated that the transferring preference for the [1,2]-shift component of the tandem reaction is methyl < ethyl. Our conclusion kept in line with the experimental work of Driver.[35]

■ ASSOCIATED CONTENT

Supporting Information

Detailed molecular coordinates of all optimized structures. This material is available free of charge via the Internet at http://pubs.acs.org.

■ AUTHOR INFORMATION

Corresponding Author

* E-mail: qinghua.ren@shu.edu.cn. Tel: +86-21-66132404. Fax: +86-21-66134594.

Notes

The authors declare no competing financial interest.

■ ACKNOWLEDGMENTS

This work is supported by Shanghai Higher Education Connotation Construction "085" Project, "Materials Genome Engineering" Funding (B.58-B111-12-101, B.58-B111-12-103), and the high-performance computing platform of Shanghai University. Q.R. is grateful for the help of Prof. Gabriel G. Balint-Kurti of the University of Bristol.

■ REFERENCES

(1) Selander, N.; Szabo, K. J. *Chem. Rev.* **2011**, *111*, 2048−2076.
(2) Rosen, B. M.; Quasdorf, K. W.; Wilson, D. A.; Zhang, N.; Resmerita, A. M.; Garg, N. K.; Percec, V. *Chem. Rev.* **2011**, *111*, 1346−1416.
(3) Arockiam, P. B.; Bruneau, C.; Dixneuf, P. H. *Chem. Rev.* **2012**, *112*, 5879−5918.
(4) Allen, S. E.; Walvoord, R. R.; Padilla-Salinas, R.; Kozlowki, M. C. *Chem. Rev.* **2013**, *113*, 6234−6458.
(5) Bolm, C.; Legros, J.; Le Paih, J.; Zani, L. *Chem. Rev.* **2004**, *104*, 6217−6254.
(6) Sherry, B. D.; Furstner, A. *Acc. Chem. Res.* **2008**, *41*, 1500−1511.
(7) Czaplik, W. M.; Mayer, M.; Cvengros, J.; von Wangelin, A. J. *ChemSusChem* **2009**, *2*, 396−417.
(8) Sun, C.; Li, B.; Shi, Z. *Chem. Rev.* **2011**, *111*, 1293−1314.
(9) Gopalaiah, K. *Chem. Rev.* **2013**, *113*, 3248−3296.
(10) Bauer, E. B. *Curr. Org. Chem.* **2008**, *12*, 1341−1369.
(11) Espino, C. G.; Fiori, K. W.; Kim, M.; Du Bois, J. *J. Am. Chem. Soc.* **2004**, *126*, 15378−15379.
(12) Lebel, H.; Huard, K.; Lectard, S. *J. Am. Chem. Soc.* **2005**, *127*, 14198−14199.
(13) Reed, S. A.; White, M. C. *J. Am. Chem. Soc.* **2008**, *130*, 3316−3318.
(14) Kim, J. Y.; Park, S. H.; Ryu, J.; Cho, S. H.; Kim, S. H.; Chang, S. *J. Am. Chem. Soc.* **2012**, *134*, 9110−9113.
(15) Hennessy, E. T.; Betley, T. A. *Science* **2013**, *340*, 591−595.
(16) Roizen, J. L.; Harvey, M. E.; Du Bois, J. *Acc. Chem. Res.* **2012**, *45*, 911−922.
(17) Cho, S. H.; Kim, J. Y.; Kwak, J.; Chang, S. *Chem. Soc. Rev.* **2011**, *40*, 5068−5083.
(18) Shou, W. G.; Li, J.; Guo, T.; Lin, Z.; Jia, G. *Organometallics* **2009**, *28*, 6847−6954.
(19) Long, A. K. M.; Timmer, G. H.; Pap, J. S.; Snyder, J. L.; Yu, R. P.; Berry, J. F. *J. Am. Chem. Soc.* **2011**, *133*, 13138−13150.
(20) Nishioka, Y.; Uchida, T.; Katsuki, T. *Angew. Chem., Int. Ed.* **2013**, *52*, 1739−1742.

DOI: 10.1021/acs.organomet.5b00087
Organometallics 2015, 34, 1129−1136

(21) Grohmann, C.; Wang, H.; Glorius, F. *Org. Lett.* **2013**, *15*, 3014−3017.
(22) Shen, M.; Leslie, B. E.; Driver, T. G. *Angew. Chem., Int. Ed.* **2008**, *47*, 5056−5059.
(23) Stokes, B. J.; Dong, H.; Leslie, B. E.; Pumphrey, A. L.; Driver, T. G. *J. Am. Chem. Soc.* **2007**, *129*, 7500−7501.
(24) Ragaini, F.; Penoni, A.; Gallo, E.; Tollari, S.; Li Gotti, C.; Lapadula, M.; Mangioni, E.; Cenini, S. *Chem.—Eur. J.* **2003**, *9*, 249−259.
(25) King, E. R.; Sazama, G. T.; Betley, T. A. *J. Am. Chem. Soc.* **2012**, *134*, 17858−17861.
(26) Sun, K.; Sachwani, R.; Richert, K. J.; Driver, T. G. *Org. Lett.* **2009**, *11*, 3598−3601.
(27) Ryu, J.; Kwak, J.; Shin, K.; Lee, D.; Chang, S. *J. Am. Chem. Soc.* **2013**, *135*, 12861−12868.
(28) He, H.; Liu, W.; Dai, L.; You, S. *J. Am. Chem. Soc.* **2009**, *131*, 8346−8347.
(29) Dong, H.; Shen, M.; Redford, J. E.; Stokes, B. J.; Pumphrey, A. L.; Driver, T. G. *Org. Lett.* **2007**, *9*, 5191−5194.
(30) Bräse, S.; Gil, C.; Knepper, K.; Zimmermann, V. *Angew. Chem., Int. Ed.* **2005**, *44*, 5188−5240.
(31) Jones, J. E.; Ruppel, J. V.; Gao, G.-Y.; Moore, T. M.; Zhang, X. P. *J. Org. Chem.* **2008**, *73*, 7260−7265.
(32) Ruppel, J. V.; Jones, J. E.; Huff, C. A.; Kamble, R. M.; Chen, Y.; Zhang, X. P. *Org. Lett.* **2008**, *10*, 1995−1998.
(33) Stokes, B. J.; Liu, S.; Driver, T. G. *J. Am. Chem. Soc.* **2011**, *133*, 4702−4705.
(34) Nguyen, Q.; Sun, K.; Driver, T. G. *J. Am. Chem. Soc.* **2012**, *134*, 7262−7265.
(35) Nguyen, Q.; Nguyen, T.; Driver, T. G. *J. Am. Chem. Soc.* **2013**, *135*, 620−623.
(36) Zhang, Q.; Wu, C.; Zhou, L.; Li, J. *Organometallics* **2013**, *32*, 415−426.
(37) Becke, A. D. *Phys. Rev. A* **1988**, *38*, 3098−3100.
(38) Becke, A. D. *J. Chem. Phys.* **1993**, *98*, 5648−5652.
(39) Lee, C. T.; Yang, W. T.; Parr, R. G. *Phys. Rev. B* **1988**, *37*, 785−789.
(40) Stephens, P. J.; Devlin, F. J.; Chabalowski, C. F.; Frisch, M. J. *J. Phys. Chem.* **1994**, *98*, 11623−11627.
(41) Krishnan, R.; Binkley, J. S.; Seeger, R.; Pople, J. A. *J. Chem. Phys.* **1980**, *72*, 650−654.
(42) McLean, A. D.; Chandler, G. S. *J. Chem. Phys.* **1980**, *72*, 5639−5648.
(43) Andrae, D.; Haussermann, U.; Dolg, M.; Stoll, H.; Preuss, H. *Theor. Chim. Acta* **1990**, *77*, 123−141.
(44) Cossi, M.; Rega, N.; Scalmani, G.; Barone, V. *J. Comput. Chem.* **2003**, *24*, 669−681.
(45) Frisch, M. J.; et al. *Gaussian 03*, version 01; Gaussian, Inc.; Wallingford, CT, 2004.
(46) Hamon, P.; Toupet, L.; Hamon, J. R.; Lapinte, C. *Organometallics* **1992**, *11*, 1429−1431.
(47) Yao, Z.; Klabunde, K. J.; Asirvatham, A. S. *Inorg. Chem.* **1995**, *34*, 5289−5294.
(48) Gusev, D. G.; Hubener, R.; Burger, P.; Orama, O.; Berke, H. *J. Am. Chem. Soc.* **1997**, *119*, 3716−3731.
(49) Daida, E. J.; Peters, J. C. *Inorg. Chem.* **2004**, *43*, 7474−7485.
(50) McQuaid, K. M.; Sames, D. J. *J. Am. Chem. Soc.* **2009**, *131*, 402−403.
(51) Murarka, S.; Deb, I.; Zhang, C.; Seidel, D. J. *J. Am. Chem. Soc.* **2009**, *131*, 13226−13227.
(52) Haibach, M. C.; Deb, I.; De, C. K.; Seidel, D. J. *J. Am. Chem. Soc.* **2011**, *133*, 2100−2103.
(53) Vukovic, J.; Goodbody, A. E.; Kutney, J. P.; Misawa, M. *Tetrahedron* **1988**, *44*, 325−331.
(54) Ishikawa, H.; Colby, D. A.; Seto, S.; Va, P.; Tam, A.; Kakei, H.; Rayl, T. J.; Hwang, I.; Boger, D. L. *J. Am. Chem. Soc.* **2009**, *131*, 4904−4916.
(55) Oestreich, M.; Hartmann, E.; Mewald, M. *Chem. Rev.* **2013**, *113*, 402−441.
(56) Marinetti, A.; Jullien, H.; Voituriez, A. *Chem. Soc. Rev.* **2012**, *41*, 4884−4908.
(57) Kozuch, S.; Shaik, S. *Acc. Chem. Res.* **2011**, *44*, 101−110.
(58) Uhe, A.; Kozuch, S.; Shaik, S. *J. Comput. Chem.* **2011**, *32*, 978−985.

DOI: 10.1021/acs.organomet.5b00087
Organometallics 2015, 34, 1129−1136